blood

2012 120: 1254-1261
Prepublished online June 18, 2012;
doi:10.1182/blood-2012-02-410407

The folliculin-FNIP1 pathway deleted in human Birt-Hogg-Dubé syndrome is required for murine B-cell development

Masaya Baba, Jonathan R. Keller, Hong-Wei Sun, Wolfgang Resch, Stefan Kuchen, Hyung Chan Suh, Hisashi Hasumi, Yukiko Hasumi, Kyong-Rim Kieffer-Kwon, Carme Gallego Gonzalez, Robert M. Hughes, Mara E. Klein, Hyoungbin F. Oh, Paul Bible, Eileen Southon, Lino Tessarollo, Laura S. Schmidt, W. Marston Linehan and Rafael Casellas

Blood (print ISSN 0006-4971, online ISSN 1528-0020), is published weekly by the American Society of Hematology, 2021 L St, NW, Suite 900, Washington DC 20036.

The folliculin-FNIP1 pathway deleted in human Birt-Hogg-Dubé syndrome is required for murine B-cell development

Masaya Baba,[1] Jonathan R. Keller,[2] Hong-Wei Sun,[3] Wolfgang Resch,[4] Stefan Kuchen,[4] Hyung Chan Suh,[2] Hisashi Hasumi,[1] Yukiko Hasumi,[1] Kyong-Rim Kieffer-Kwon,[4] Carme Gallego Gonzalez,[5] Robert M. Hughes,[1] Mara E. Klein,[1] Hyoungbin F. Oh,[1] Paul Bible,[3] Eileen Southon,[6] Lino Tessarollo,[7] Laura S. Schmidt,[1,6] *W. Marston Linehan,[1] and *Rafael Casellas[4,8]

[1]Urologic Oncology Branch, National Cancer Institute (NCI), National Institutes of Health (NIH), Bethesda, MD; [2]Laboratory of Cancer Prevention, NCI, NIH, Frederick, MD; [3]Biodata Mining and Discovery Section, National Institute of Arthritis and Musculoskeletal and Skin Diseases (NIAMS), NIH, Bethesda, MD; [4]Genomics & Immunity, NIAMS, NCI, NIH, Bethesda, MD; [5]Institut de Biologia Molecular de Barcelona, Barcelona, Spain; [6]Basic Science Program, SAIC-Frederick, NCI-Frederick, Frederick, MD; [7]Mouse Cancer Genetics Program, Center for Cancer, NCI-Frederick, Frederick, MD; and [8]Center for Cancer Research, NCI, NIH, Bethesda, MD

Birt-Hogg-Dubé (BHD) syndrome is an autosomal dominant disorder characterized by cutaneous fibrofolliculomas, pulmonary cysts, and kidney malignancies. Affected individuals carry germ line mutations in folliculin (*FLCN*), a tumor suppressor gene that becomes biallelically inactivated in kidney tumors by second-hit mutations. Similar to other factors implicated in kidney cancer, FLCN has been shown to modulate activation of mammalian target of rapamycin (mTOR). However, its precise in vivo function is largely unknown because germ line deletion of *Flcn* results in early embryonic lethality in animal models. Here, we describe mice deficient in the newly characterized folliculin-interacting protein 1 (Fnip1). In contrast to *Flcn*, *Fnip1*$^{-/-}$ mice develop normally, are not susceptible to kidney neoplasia, but display a striking pro-B cell block that is entirely independent of mTOR activity. We show that this developmental arrest results from rapid caspase-induced pre-B cell death, and that a Bcl2 transgene reconstitutes mature B-cell populations, respectively. We also demonstrate that conditional deletion of *Flcn* recapitulates the pro-B cell arrest of *Fnip1*$^{-/-}$ mice. Our studies thus demonstrate that the FLCN-FNIP complex deregulated in BHD syndrome is absolutely required for B-cell differentiation, and that it functions through both mTOR-dependent and independent pathways. (*Blood*. 2012;120(6):1254-1261)

Introduction

Human Birt-Hogg-Dubé (BHD) syndrome is an autosomal dominant hereditary cancer syndrome characterized by the development of cutaneous fibrofolliculoma, multiple pulmonary cysts, spontaneous pneumothorax, and increased risk of renal cell neoplasia.[1,2] Affected individuals carry germ line mutations in *FLCN*, a recently characterized gene that encodes a 64-kDa protein, folliculin.[2] In kidney tumors, the *FLCN* wild-type (WT) allele is deleted by somatic mutation or loss of heterozygosity,[3-5] supporting the idea that *FLCN* is a classic tumor suppressor gene that follows the Knudson 2-hit hypothesis.[6] *FLCN* lacks predicted functional domains or homology to known proteins; however, it is also highly conserved across species indicating that it might play an essential role in development.[2] In agreement with this notion, homozygous loss of *Flcn* in mice causes visceral endoderm defects and embryonic lethality at E5.5-E6.5.[5]

Although its precise in vivo function is unknown, folliculin may regulate cellular energy sensing by controlling mTOR signaling.[7-10] For instance, loss of *Flcn* in mouse kidneys leads to cellular hyperproliferation and overactivation of mTORC1, mTORC2, and MAPK pathways, whereas rapamycin treatment partially rescues this phenotype.[5,11-14] In this context, *FLCN* is not unlike the 6 additional genes that have so far been implicated in kidney cancer (*VHL*, *MET*, *TSC1*, *TSC2*, *FH*, and *SDH*), in that they all interact with metabolic pathways that respond to stress or nutrient stimulation (reviewed by Linehan et al[15]). However, mounting evidence indicates that folliculin may also regulate additional signal transduction pathways independent of mTOR activity. *Flcn*$^{-/-}$ embryonic stem (ES) cells for instance are resistant to apoptosis as a result of aberrant transforming growth factor (TGF)β signaling.[14] In kidney cell lines, *FLCN* deficiency results in increased activity of TFE3, a member of the MiTF/TFE transcription factor family.[16] Furthermore, deletion of the FLCN homolog in fruit flies disrupts male germ line stem cell maintenance, a defect that appears to be linked to the JAK/STAT (Janus kinase/signal transducer and activator of transcription) pathway.[17]

Two folliculin interacting proteins, FNIP1 and FNIP2, were recently isolated.[7-9] These factors are broadly expressed in human tissues and specifically associate with folliculin C-terminal domain in ex vivo studies.[7-9] The significance of this interaction is implicit by the fact that most BHD-causing mutations delete the folliculin C-terminal domain.[1] Further supporting the link between BHD syndrome and mTOR signaling, the FLCN-FNIP complex has been shown to interact with and be phosphorylated by 5′-adenosine monophosphate (AMP)–activated protein kinase (AMPK), a key enzyme in cellular energy sensing that negatively regulates mTOR activity.[11] However, whether FNIP proteins are true functional

Submitted February 13, 2012; accepted June 6, 2012. Prepublished online as *Blood* First Edition paper, June 18, 2012; DOI 10.1182/blood-2012-02-410407.

*W.M.L. and R.C. contributed equally to this work.

The online version of this article contains a data supplement.

The publication costs of this article were defrayed in part by page charge payment. Therefore, and solely to indicate this fact, this article is hereby marked "advertisement" in accordance with 18 USC section 1734.

partners of FLCN in vivo and are thus implicated in BHD syndrome has not been directly established.

Here, we report the analysis of *Fnip1* knockout (KO) mice. In contrast to *Flcn*$^{-/-}$, we show that *Fnip1* germ line targeting does not lead to embryonic lethality or kidney hyperplasia. Unexpectedly, the mice display a marked pro-B cell arrest (the Hardy fraction C-C′), which unlike tumor development in BHD mice, cannot be rescued by rapamycin treatment and is thus mTOR independent. Transcriptome analyses of *Fnip1*$^{-/-}$ pro-B cells reveal compromised expression of key genes implicated in B-cell surface expression, including *VpreB1*/*VpreB2*, *λ5*, and *Rag1*/*Rag2*. We also show that expression of prerecombined heavy and light-chain genes in *Fnip1*$^{-/-}$ mice helps bypass the pro-B cell arrest to the transitional bone marrow (BM) IgM^{+} compartment. Strikingly, the reconstituted immature B cells fail to migrate to the periphery. We show that this block is driven by caspase activation and intrinsic cell death, and that expression of a Bcl2 antiapoptotic transgene promotes normal numbers of peripheral B cells in the knockout. Finally, in support of an in vivo functional link between *Flcn* and *Fnip1*, we show that tamoxifen-inducible deletion of folliculin in mice recapitulates the *Fnip1*$^{-/-}$ pro-B cell arrest.

We conclude that (1) the folliculin/Fnip pathway mutated in BHD syndrome is strictly required for BM B-cell survival, (2) folliculin works through both mTOR-dependent (ie, kidney tumor development) and independent (ie, B-cell developmental arrest) mechanisms, and (3) *Fnip1*$^{-/-}$ mice phenocopy a subset of abnormalities associated with *Flcn* deletion.

Methods

Gene targeting and drug treatments

Fnip1 gene-trap ES cells (RRM154) were purchased from BayGenomics. In this clone, the gene-trap vector (pGT0Lxf) carrying a splice-acceptor sequence was inserted within intron 2. ES cells were injected into C57BL/6J blastocysts. After germ line transmission mice were backcrossed to the C57BL/6J background for 3 generations. The *Fnip1*^{lox} allele was introduced by targeting a neomycin resistance cassette (Neo^{r}), flanked by Frt and loxP sequences, into *Fnip1* intron 5. A second loxP sequence was inserted within intron 6. The targeting vector also carried a thymidine kinase gene for negative selection. ES cells were selected for G418 resistance and gancyclovir sensitivity. Proper targeting was assessed by Southern blotting. Backcrossing of chimeras to C57BL/6J mice produced heterozygous F1 offspring with germ line transmission of the *Fnip1* floxed (f) allele. The Neo cassette flanked by *Frt* sites was excised in vivo by a *Flp* recombinase transgene expressed under the β-actin promoter.[18] To generate a *Fnip1* deleted allele (*Fnip1*$^{+/-}$), a β-actin-Cre recombinase transgene[19] was introduced into *FNIP1*$^{f/+}$ mice, followed by backcrossing to the C57BL/6J for Cre transgene removal. The *Flcn* conditional knockout allele was previously described.[11] To conditionally delete the *Flcn*^{f} allele, a *CreER* transgene[20] was introduced into *Flcn*$^{f/-}$ mice, and at 6 weeks of age *Flcn*$^{f/-}$*CreER* mice were intraperitoneally injected with tamoxifen dissolved in corn oil at the dosage of 130 mg/kg. For rapamycin treatment, rapamycin (LC Laboratories) was dissolved in 100% ethanol at a stock concentration of 10 mg/mL and kept at −20°C. Rapamycin stock solution was diluted to 200 μg/mL in buffer (5% Tween 80, 5% PEG400) and injected intraperitoneally at a dose of 2 mg/kg daily. Animal care procedures followed National Cancer Institute (NCI)–Frederick Animal Care and Use Committee guidelines.

Flow cytometry

With the exception of IgM-Cy5 (Jackson ImmunoResearch Laboratories), antibodies were from BD Bioscience: B220-PercP-Cy5.5, B220-APC, CD4-PE, CD8-FITC, CD43-FITC, CD43-PE, CD19-APC, CD19-PercP-Cy5.5, CD24-FITC, BP-1-biotin, CD25-APC, CD25-PE, Igκ-PE, CCR9-PE, streptavidin-APC, and FcR. Dead cells were gated using DAPI (Sigma-Aldrich) or TO-PRO-3. Flow cytometers were FACSCalibur (BD Bioscience) and CyanADP (Beckman Coulter), and as cell sorter we used BD Bioscience FACSAriaII. Flow cytometry analysis was done with FlowJo Version 9.4.10 software (TreeStar). Intracellular staining was performed using BD Cytofix/Cytoperm fixation/permeabilization kit. For apoptotic cell detection, Vybrant FAM poly caspase assay kit (Molecular Probes) was used with DAPI according to the manufacturer's protocol.

qRT-PCR

Total RNA was isolated with TRIzol (Invitrogen) and reverse transcribed using Superscript III reverse transcriptase kit (Invitrogen). Quantitative PCR (qPCR) was performed via 7300 Realtime PCR System (Applied Biosystems) using SYBR Green PCR Master Mix (Fermentas). Relative gene expression was measured by normalizing Ct values based on expression of *Rplp0* (*36B4*) gene control. PCR primer sequences are provided as supplemental Methods (available on the *Blood* Web site; see the Supplemental Materials link at the top of the online article).

mRNA-Seq

BM cells from *FNIP1*$^{+/+}$ and *FNIP1*$^{-/-}$ mice were stained with CD24(heat shock antigen)–FITC, CD43−PE, B220-PerCP-Cy5.5, and BP-1-APC. Fraction B (B220^{low}CD43^{+}CD24^{+}BP-1^{-}) and Fraction C-C′ (B220^{low}CD43^{+}CD24^{+}BP-1^{+}) pro-B cells were sorted and mRNA libraries were generated according to the mRNA TrueSeq sample prep kit (Illumina), sequenced on a HiSeq 2000 (Illumina) and analyzed as previously described.[21]

Western blotting

Kidney tissues were flash-frozen in liquid nitrogen immediately after dissection. Frozen tissues were homogenized by polytron homogenizer on ice in radio immunoprecipitation assay (RIPA) buffer (20mM tris-HCl, pH 7.5, 150mM NaCl, 1mM ethylenediaminetetraacetic acid, 1.0% Triton X-100, 0.5% deoxycholate, 0.1% sodium dodecylsufate, PhosSTOP [Roche], phosphatase inhibitor cocktail [Roche], and complete protease inhibitor cocktail [Roche]), followed by centrifugation at 13 200g for 30 minutes. Protein concentrations of cleared supernatants were measured with BCA protein assay kit (Pierce) and adjusted to 1.33 mg/mL. Four times SDS sample buffer was then added and samples were boiled for 5′ to produce 1 mg/mL sample lysates. A total of 20 μg of protein was loaded onto 4% to 20% tris-glycin SDS-PAGE gels. Immunoblotting was performed as previously described [11] with minor modifications optimized for Odyssey infrared imaging system (LI-COR). In brief, separated proteins were transferred to Immobilon-FL polyvinylidene difluoride (PVDF) membrane (Millipore), blocked with Odysey blocking buffer (LI-COR) at room temperature for 1 hour. Blocked membranes were incubated overnight at 4°C with primary antibodies, diluted with 0.1% bovine serum albuminTris-buffered saline with Tween 20 (TBST; 20mM Tris-HCl pH8.0, 150mM NaCl, 0.05% Tween 20) as follows: p-mTOR (Ser2448) 1:1000, p-mTOR (Ser2448) 1:1000, mTOR 1:1000, p-S6 ribosomal protein (Ser240/244) 1:1000, p-S6 ribosomal protein (Ser235/236) 1:1000, S6 ribosomal protein 1:1000, and GAPDH (glyceraldehyde-3-phosphate dehydrogenase) 1:1000. All antibodies were purchased from Cell Signaling. After 3 washes with TBST, membranes were incubated at room temperature for 1 hour with infrared dyes conjugated secondary antibody IRDye 800CW goat anti–rabbit IgG (LI-COR), diluted 1:15 000 with 0.2% Tween 20/Odysey blocking Buffer. After 3 additional washes with TBST and brief soaking in phosphate-buffered saline, images were acquired with an Odyssey infrared imaging system (LI-COR).

V(D)J recombination

Sorted C/C′ fraction cells were digested with proteinase K. Digested solution was directly used for PCR after heat inactivation of proteinase K. D-J and V-DJ recombination events were amplified by PCR using primers and conditions as previously described.[22] PCR products were separated on agarose gels, transferred to a membrane and analyzed by Southern blot using published oligonucleotide probes.[22]

Figure 1. Generation of *Fnip1* KO mice. Left schematics show *Fnip1* WT (*Fnip1*$^{+}$), targeted (*Fnip1*^{lox}), and gene-trapped (*Fnip1*$^{\beta\text{-}Geo}$) alleles. The *Fnip1*^{lox} mutation was introduced in the germ line by targeting a neomycin resistance cassette (flanked by LoxP sites) within intron 5, followed by a second LoxP site within intron 6. The Neo-exon 6 sequence was removed by crossing targeted mice with β-actin-Cre transgenic mice.[19] Exon 6 deletion generates a premature termination codon in exon 7. *Fnip1*$^{\beta\text{-}Geo}$ mice were derived from GeneTrap ES cell clone RRM154, which carries a splice acceptor (SA) β-Geo cassette inserted within intron 2. Proper gene targeting in both cases was confirmed by Southern blotting (right gel pictures).

Statistical analysis

All the statistical analysis were performed with the Mann Whitney *U* test or Student *t* test as appropriate, and represented as mean ± SD. *P* values were defined as: $P < .05$; $P < .01$; NS (nonsignificant) $P > .05$.

Results

Intrinsic pro-B to pre-B cell block in *Fnip1*$^{-/-}$ mice

To determine the in vivo function of Fnip1, we targeted the *Fnip1* gene in the mouse germ line (Figure 1, *Fnip1*^{lox}). In parallel, we generated a second *Fnip1* knockout line using GeneTrap ES cells (IGTC clone RRM154, Figure 1, *Fnip1β-Geo*). As no phenotypic differences were observed between the 2 lines, we used them interchangeably throughout the studies and they will be referred to hereafter as *Fnip1*$^{-/-}$ mice. In contrast to *Flcn*,[5] deletion of *Fnip1* did not compromise viability or fertility, as progeny from heterozygous crosses were born in normal Mendelian ratios (not shown). Unexpectedly, gross anatomical inspection showed a significant reduction in the spleen size of *Fnip1* KO mice compared with heterozygous or WT controls ($P < .01$, Figure 2A left graph). To examine whether this feature was the result of defective lymphopoiesis we analyzed BM, thymus, and spleen from all 3 strains by flow cytometry. We found that total thymocyte numbers and peripheral T cells were normal in the absence of Fnip1 (Figure 2B). In agreement with this observation, thymus size was comparable between knockout and littermate controls (Figure 2A right graph). In contrast, *Fnip1*$^{-/-}$ mice were severely B-cell lymphopenic, in that they displayed a nearly complete lack of conventional splenic CD19^{+} cells (Figure 2C). Similarly, B220^{low}CD19^{high} peritoneal B1 cells were depleted in the knockout (Figure 2D). In the BM, B220^{high} mature recirculating, B220^{low}IgM^{high} transitional, and B220^{low}CD43^{-}CD25^{+} pre-B cells were also markedly reduced in *Fnip1*$^{-/-}$ mice (Figure 2E-G and not shown). Conversely, there was a consistent accumulation of B220^{low}CD43^{+}CD25$-$pro-B cells in mutant mice, as their absolute number was 2- to 3-fold increased relative to control ($P < .05$, Figure 2E-G).

To precisely define the B-cell population(s) affected by the absence of Fnip1, we fractionated B220^{low}CD43^{+} pro-B cells into the Hardy A, B, C, and C′ subsets based on differential cell-surface expression of HSA and BP-1.[23] We found that relative to control, there was a clear accumulation of pro-B cell fractions C and C′ in *Fnip1*-deficient mice (Figure 2H). Outside the B-cell compartment, BM monocyte (Mac-1^{+}Gr-1^{-}), granulocyte (Mac-1^{+}Gr-1^{+}), and erythrocyte (CD71^{+}Ter119^{+}) lineages appeared normal (not shown). On the basis of these findings we conclude that germ line deletion of *Fnip1* leads to a specific developmental block at pro-B cell fractions C-C′.

To explore whether the *Fnip1*$^{-/-}$ B-cell lymphopenia was the result of cell autonomous or environmental abnormalities we performed BM transplantation experiments. We found that whereas *Fnip1*$^{+/-}$ donor BM cells reconstituted the B-cell compartment of irradiated Ly5.2 congenic mice, transplanted *Fnip1*$^{-/-}$ cells recapitulated the same pro-B cell developmental arrest observed in *Fnip1*$^{-/-}$ mice. Conversely, T cells and other hematopoietic lineages were equally reconstituted in the 2 strains (not shown). We conclude that the B lymphocyte defect of Fnip1 deficient mice is cell intrinsic.

Fnip1$^{-/-}$ mice recapitulate some but not all *Flcn*$^{-/-}$ defects

We sought to ascertain whether folliculin deficiency was also associated with a pro-B cell defect. Because *Flcn* germ line deletion is embryonic lethal,[5] we generated *Flcn*$^{flox/-}$ mice expressing Cre-ER fusion recombinase under the pCAGGS promoter (CreER).[20] Six-week-old mice were injected with 1 dose of tamoxifen (130 mg/kg) and BM, spleen, and thymuses were analyzed by flow cytometry 4 or 8 weeks after treatment. Consistent with the *Fnip1*$^{-/-}$ phenotype, *Flcn*$^{flox/-}$CreER mice showed few CD19^{+} B cells in the spleen and displayed a pro-B cell block in the BM (Figure 3A and not shown). Thus, conditional *Flcn* deletion phenocopies the B-cell developmental defect observed in *Fnip1*$^{-/-}$ mice.

Analogous to other factors that suppress kidney cancer, folliculin interacts with the energy and nutrient sensing AMPK-mTOR signaling pathway,[5] the target of rapamycin. In support of this, *Flcn* deletion in kidneys results in mTOR overactivation (hyperphosphorylation), uncontrolled kidney cell proliferation, polycystic kidneys, and death from renal failure by 3 weeks of age.[11] Rapamycin treatment on the other hand suppresses uncontrolled kidney cell proliferation and significantly extends median survival.[11] In contrast to *Flcn*$^{-/-}$, we detected few or no cysts in *Fnip1*$^{-/-}$ kidneys (Figure 3B), and there was no renal failure in the absence of Fnip1 (not shown), implying that mTOR activity was unaffected in the absence of Fnip1. To directly assess mTOR activation in *Fnip1*$^{-/-}$ mice we measured phosphorylation of both mTOR (Ser2448 and Ser2481) and one of its downstream targets, the S6 subunit of the 40S ribosomal complex (Ser235/236 and Ser240/244). As previously shown,[5,7] both proteins were hyperphosphorylated in *Flcn* deleted kidney cells (Figure 3C). Conversely, the levels of mTOR and S6 phosphorylation in kidney or pro-B cells were comparable between *Fnip1*$^{-/-}$ and littermate controls (Figure 3C and not shown), demonstrating that mTOR signaling is not compromised

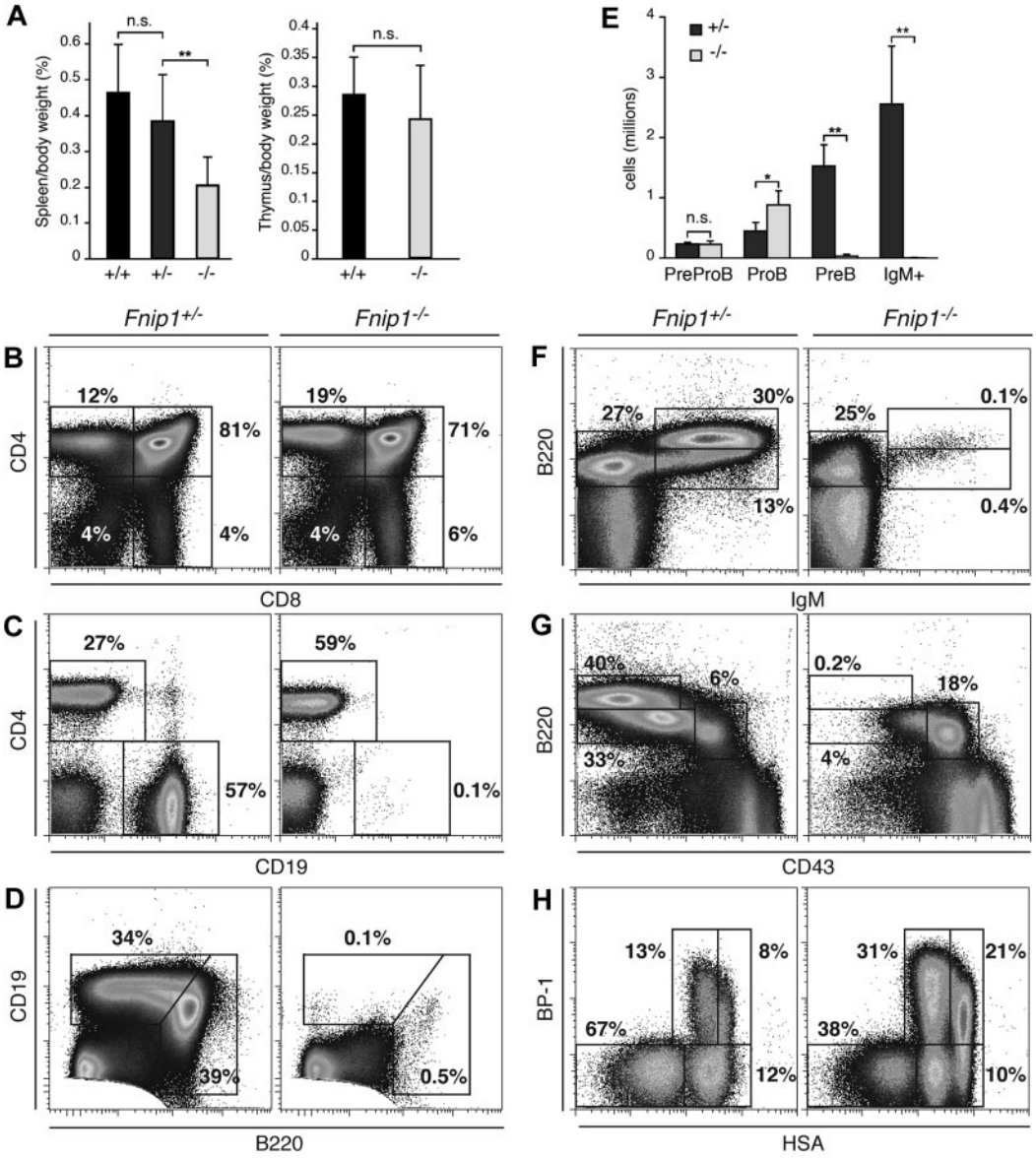

Figure 2. Severe pro-B cell arrest in *Fnip1*$^{-/-}$ mice. (A) Left bar graph: spleen weight (given as percentage of body weight) in *Fnip1*$^{-/-}$ mice relative to littermate controls graphed as the mean ± SD; NS = no statistical significance, $^{**}P < .01$ (Student *t* test), n = 9 (*Fnip1*$^{+/+}$), 17 (*Fnip1*$^{+/-}$), and 13 (*Fnip1*$^{-/-}$). Right graph shows the same for thymuses. n = 6 (*Fnip1*$^{+/+}$), and 8 (*Fnip1*$^{-/-}$). (B-D) Fluorocytometric analysis of CD4$^+$ and CD8$^+$ thymocytes (B), CD4$^+$ and CD19$^+$ splenocytes (C), and B1 (B220^{high}CD19^{low}) and B2 (B220^{low}CD19^{high}) peritoneal cavity B cells (D). (E) Absolute number of pre–pro-B (B220$^+$IgM$^-$CD19$^-$), pro-B (B220$^+$IgM$^-$CD19$^+$CD43$^+$CD25$^-$), pre-B (B220$^+$IgM$^-$CD19$^+$CD43$^-$CD25$^+$), and immature (B220$^+$IgM$^+$) B cells in BM of *Fnip1*$^{+/-}$ and *Fnip1*$^{-/-}$mice. $^{*}P < .05$, $^{**}P < .01$ (Student *t* test), n = 4 for both strains. (F-H) Fluorocytometric analysis of B220 and IgM (F), B220 and CD43 (G), and BP-1 and HSA (H) expression in BM cells from *Fnip1*$^{+/-}$and *Fnip1*$^{-/-}$mice. Each analysis is representative of at least 3 independent experiments.

by Fnip1 depletion. To confirm this result, *Fnip1*$^{-/-}$ newborn mice were injected intraperitoneally with rapamycin (2 mg/kg) or buffer control on a daily basis for a total of 3 weeks. Although rapamycin treatment clearly reverted the kidney phenotype of *Flcn*$^{-/-}$ mice[11] and decreased mTOR phosphorylation in *Fnip1*$^{-/-}$ cells (supplemental Figure 1), it could not bypass the B-cell lymphopenia of *Fnip1* deficient mice (Figure 3D). Thus the *Fnip1*$^{-/-}$ pro-B cell block is independent of mTOR signaling. Taken together the observations demonstrate that *Fnip1*$^{-/-}$ mice recapitulate some but not all developmental defects associated with *Flcn* deletion.

A pre-recombined B-cell receptor does not reconstitute *Fnip1*$^{-/-}$ B cells

To clarify the nature of the *Fnip1*$^{-/-}$ B-cell lymphopenia, we sought to compare transcription profiles of WT and mutant pro-B cells. To this end pro-B cell fractions B and C-C′ were sorted to ~95% purity and from each fraction, 2 biologic replicate transcriptomes were obtained by deep-sequencing.[21] Interestingly, with few exceptions the transcriptomes of B and C-C′ fractions were nearly identical both in WT and KO mice (Figure 4A and not shown). In contrast, *Fnip1*$^{+/+}$ and mutant cells showed significant differences in both fractions, with at least 400 transcripts displaying greater than 2 fold change between the 2 cell types (false discovery rate = 1%, Figure 4B and supplemental Table 1). Among these we found key genes implicated in B-lymphocyte development, including *Cd22*, *Cd5*, *Prkcq*, *Il10rα*, *E2f2*, *Epha2*, *Ccr9*, *Vpreb1*, *Vpreb2*, *λ5*, and *Rag1*/*Rag2*. Figure 4C shows qPCR and flow cytometric results that validate defective expression of a subset of these genes in *Fnip1*$^{-/-}$ pro-B cells.

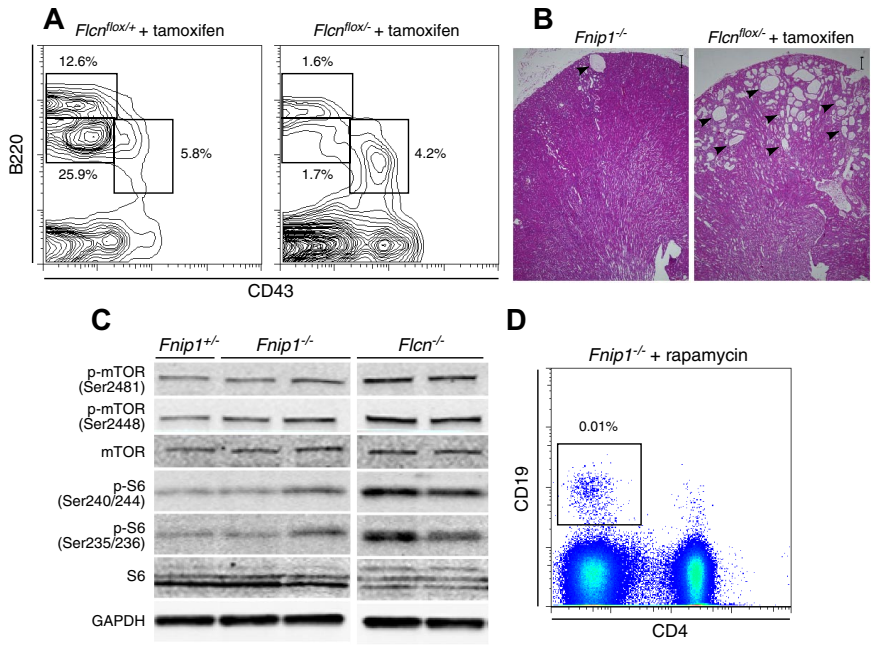

Figure 3. Comparison of *Fnip1*$^{-/-}$ and tamoxifen-induced *Flcn* deficient mice. (A) BM B-cell analysis in *Flcn*$^{f/+}$*ERCre*$^{+}$ and *Flcn*$^{f/-}$*ERCre*$^{+}$ mice 4 weeks post-tamoxifen (TM) injection. Cell samples were stained with CD43 (FITC) and B220 (PE). (B) *Flcn*$^{f/-}$*ERCre*$^{+}$ mice treated with tamoxifen (right micrograph) show hyperplastic cystic lesions (denoted with arrowheads) in kidney. Conversely, *Fnip*$^{-/-}$ mice rarely display cysts (left micrograph). Scale bar = 200 μm. (C) Western blot analysis of kidney cell lysates from *Fnip1*$^{+/-}$, *Fnip1*$^{-/-}$, and *Flcn*$^{-/-}$ mice. mTOR activation was assessed via phosphorylation of mTOR serines 2481 and 2448, as well as phosphorylation of ribosomal protein S6, serines 240/244 and 235/236. GAPDH expression was used as a loading control. (D) Failure to rescue peripheral CD19^{+} B lymphocytes in *Fnip1*$^{-/-}$ mice treated with buffer or rapamycin (2 mg/kg) for 3 weeks. Each fluorescence-activated cell sorter (FACS) analysis is representative of at least 3 independent experiments.

Because Vpreb, λ5 and Rag proteins control recombination and expression of the B-cell surface receptor we assessed intracellular Igκ and Igμ expression by flow cytometry. As expected based on the reduced number of pre-B cells, there were but background levels (< 1%) of intracellular Igκ in *Fnip1*$^{-/-}$ BM B220^{low} cells (Figure 5A). However, in spite of the pro-B cell accumulation, we also detected lower levels of intracellular Igμ within B220^{low}CD43^{+} cells in KO mice compared with controls (13% vs 24%, Figure 5B). To investigate whether V(D)J recombination is compromised in *Fnip1*$^{-/-}$ progenitor cells we cell sorted fraction C/C′ lymphocytes from KO and control mice and amplified D-J and V-DJ recombination products by PCR as described.[22] We found no significant differences in the levels of D-J recombination between the 2 strains (Figure 5C). V-DJ recombination products were also amplified from *Fnip1*$^{-/-}$ pro-B cells, although less efficiently for distal recombination events, such as V_H3609 and V_HJ558 (Figure 5C), a result perhaps explained by the reduced Rag expression in knockout cells. The data therefore show no overt defects in Rag-mediated recombination in *Fnip1*$^{-/-}$ BM B cells. Likewise, arguing against the idea that KO mice lack a pre-B cell surface receptor, flow cytometry showed λ5 staining in *Fnip1*$^{-/-}$ pro-B cells (supplemental Figure 2). Consistent with the transcriptome results, λ5+ pro-B cell numbers were modestly decreased in the knockout (supplemental Figure 2).

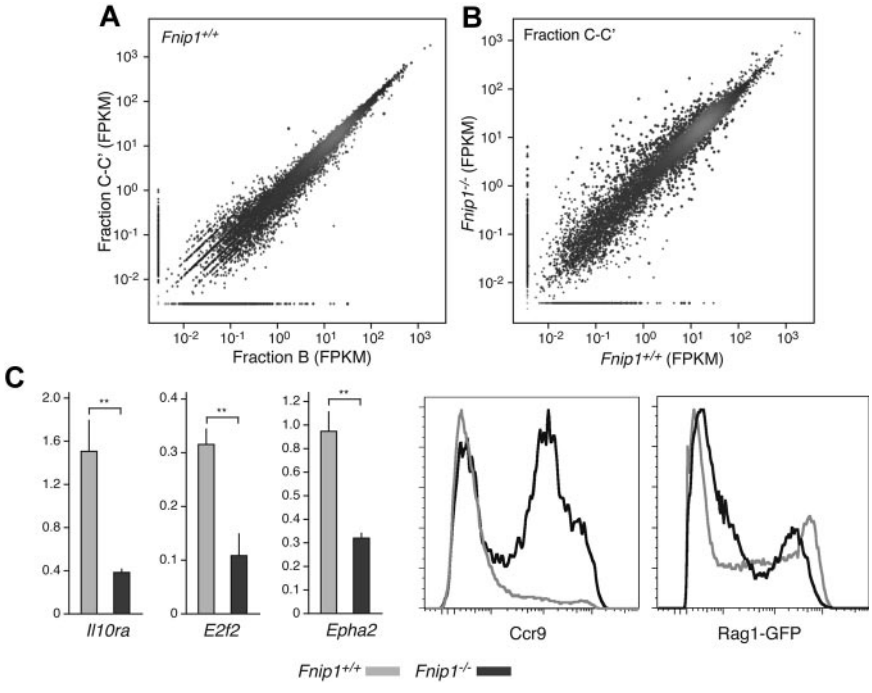

Figure 4. Transcriptome analysis of *Fnip1*$^{-/-}$ pro-B cells. (A) Scatter plot showing a comparative analysis between *Fnip1*$^{+/+}$ transcriptomes (mRNA-Seq FPKM values) obtained from the Hardy pro-B cell fractions B and C-C′. Red dots represent genes whose transcription is statistically different between the 2 fractions; n = 1 (using pooled estimates of dispersion). (B) Same analysis as in panel A but comparing fractions C-C′ between *Fnip1*$^{+/+}$ and *Fnip1*$^{-/-}$ mice; n = 2 for each genotype. (C) Bar graphs showing RT-qPCR measurements of transcription in *Fnip1*$^{+/+}$ and *Fnip1*$^{-/-}$ pro-B cells from selected genes (n = 3). Histograms showing ccr9 and Rag1-GFP expression, as determined by flow cytometry, on B220^{+}IgM^{-}CD25^{-} pro-B cells from KO and control mice. Each FACS analysis is representative of at least 3 independent experiments.

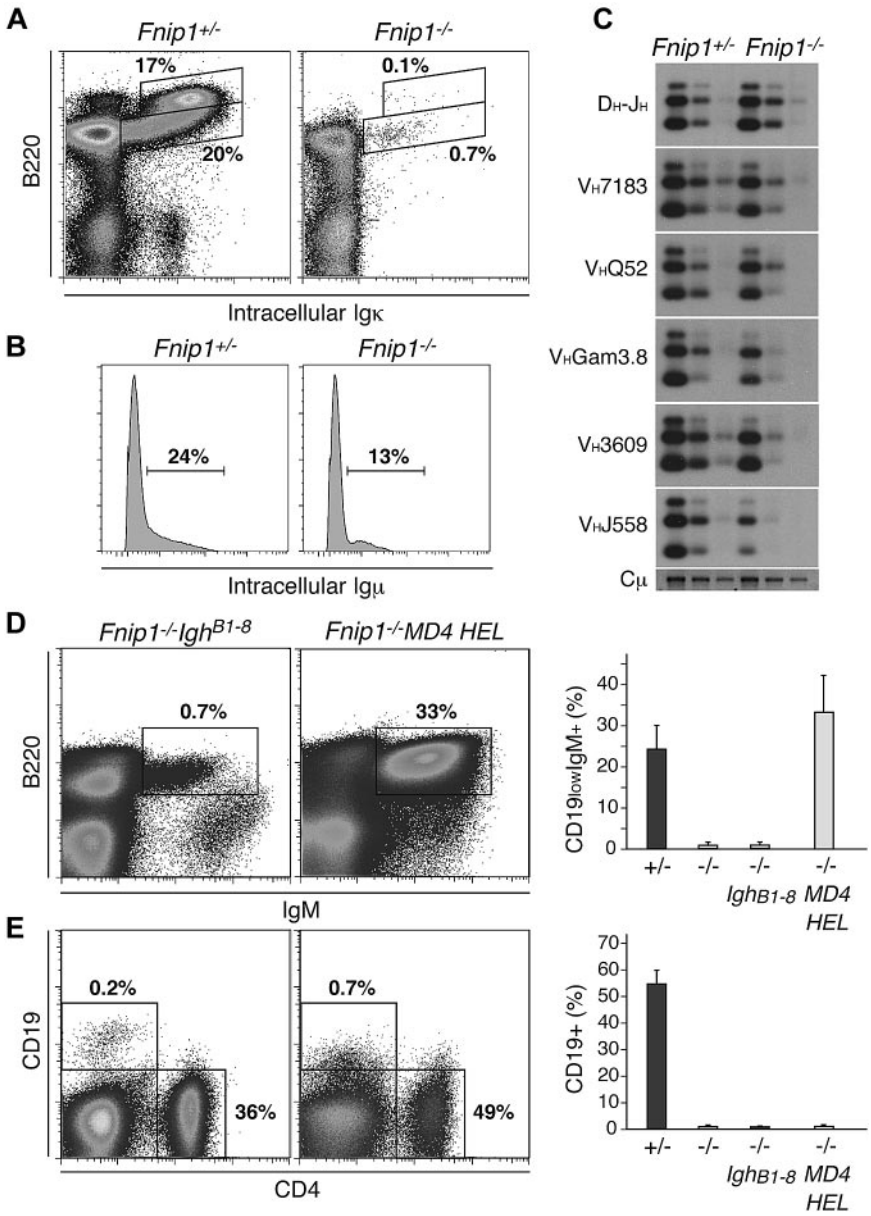

Figure 5. Prerecombined antibody genes do not rescue *Fnip1*$^{-/-}$ B cells. (A) Igκ staining in *Fnip1*$^{+/-}$ and *Fnip1*$^{-/-}$ BM B220^{+} B cells. (B) Histogram of intracellular Igμ expression in B220^{+}CD43^{+} pro-B cells from *Fnip1*$^{+/-}$ and *Fnip1*$^{-/-}$ mice. (C) D-J and V-DJ recombination analysis in WT and KO fraction C/C′ B cells as determined by PCR-Southern blot. (D) B220/IgM expression profiles in *Fnip1*$^{-/-}$ mice expressing B1-8 heavy chain (*Igh*$^{B1-8}$)[24] or the αHEL heavy and light chain transgene (*MD4 HEL*).[25] Right bar graph represents the mean ± SD of IgM^{+}B220^{+} B cells from each strain; n values were as follows: 6 for *Fnip1*$^{+/-}$ and *Fnip1*$^{-/-}$, and 3 for *Fnip1*$^{-/-}$ *Igh*$^{B1-8}$ and *Fnip1*$^{-/-}$ *MD4 HEL*. (E) Same analysis as in panel D but using CD19 and CD4 staining of splenocytes; n values: 5 mice for *Fnip1*$^{+/-}$ and *Fnip1*$^{-/-}$, and 4 mice for *Fnip1*$^{-/-}$ *Igh*$^{B1-8}$ and *Fnip1*$^{-/-}$ *MD4 HEL*. Each FACS analysis is representative of at least 3 independent experiments.

To formally exclude the possibility that defects in B-cell receptor assembly or expression might explain the *Fnip1*$^{-/-}$ B-cell phenotype, we expressed a pre-recombined heavy chain knock-in (*Igh*$^{B1-8}$,[24]), or heavy and light-chain transgenes (MD4 HEL,[25]) in *Fnip1*$^{-/-}$ mice. We found that preassembled heavy and light-chain genes (but not heavy-chain only) resulted in a substantial number of BM immature B220^{low}IgM^{+} cells in the knockout (Figure 5C middle panel and bar graph). Strikingly, in neither case did we observe peripheral splenic B2 or peritoneal B1 cells after reconstitution (Figure 5D and not shown). The findings are thus consistent with the notion that the *Fnip1*$^{-/-}$ BM B-cell block is not caused by defects in V(D)J recombination or cell-surface expression of a functional B-cell receptor.

Fnip1$^{-/-}$ pre-B cells undergo rapid apoptosis

We entertained the possibility that lack of peripheral B cells in *Fnip1*$^{-/-}$ mice might result from BM precursor cell death. Therefore we measured cell death in pro-B and pre-B cells from KO and WT controls with the fluorescent DNA stain DAPI. We found increased numbers of DAPI^{+} pro-B cells in the KO but this was not statistically significant ($P = .1$, Figure 6A). Conversely, there were on average 10 times more DAPI^{+} pre-B cells in *Fnip1*$^{-/-}$ relative to littermates ($P < .02$, Figure 6A). In addition, as determined by affinity labeling assays, deficient pre-B cells displayed enhanced caspase activity relative to Fnip1 proficient cells (Figure 6B). The results suggest that Fnip1 modulates BM B-cell survival. To confirm this idea we explored whether ectopic overexpression of antiapoptotic Bcl2 in the B-cell compartment (Eμ-Bcl2)[26] was sufficient to rescue the developmental defect associated with Fnip1 deficiency. We found that Bcl-2 expression led to increased numbers of B220^{+}IgM^{+} B cells in the BM (Figure 6C). Importantly, both splenic CD19^{+} and peritoneal B1 cell populations were reconstituted in Eμ-Bcl2 *Fnip1*$^{-/-}$ mice (Figure 6D and not shown). This was in direct contrast to the lack of peripheral B cells observed in MD4 *Fnip1*$^{-/-}$ mice (Figure 5E). We conclude that

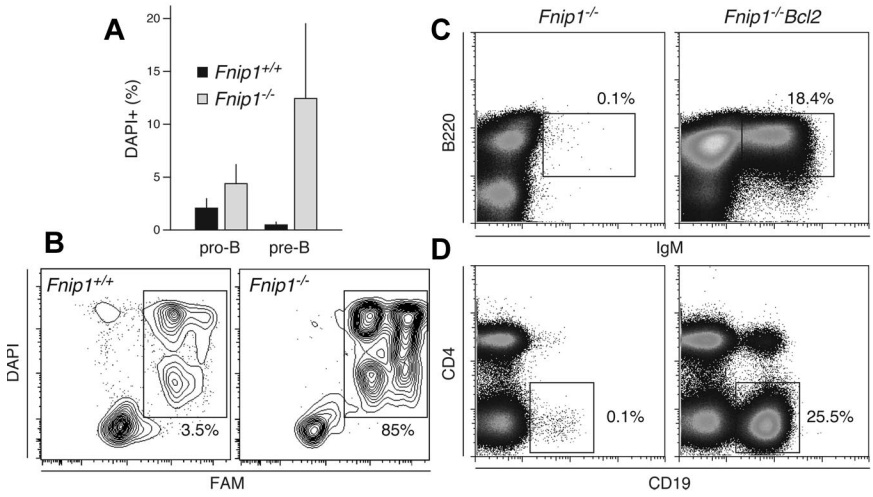

Figure 6. Increased caspase activation and apoptosis in *Fnip1*$^{-/-}$ B cells. (A) Bar graph showing the frequency of dead cells within pro-B (B220^{low}IgM^{-}CD25^{-}) and pre-B (B220^{low}IgM^{-}CD25^{+}) populations from *Fnip1*$^{+/+}$ and *Fnip1*$^{-/-}$ mice as measured by DAPI staining. Mean ± SD from 4 independent experiments, (pro-B) $P = .1$, (pre-B) $P < .02$, Student t test. (B) Flow cytometric measurement of caspase activity in *Fnip1*$^{+/+}$ and *Fnip1*$^{-/-}$ pre-B cells from interleukin 7 ex vivo cultures. Twenty-four hours after interleukin 7 removal cells were stained with DAPI and FAM, a carboxyfluorescein moiety that becomes covalently linked to the active site of caspases. (C) Flow cytometric analysis of BM and (D) spleen cells from *Fnip1*$^{-/-}$ mice reconstituted with an Eμ-Bcl2 transgene. BM cells were stained with anti-B220 and anti-IgM antibodies; staining for splenocytes was with anti-CD4 and anti-CD19. Each FACS analysis is representative of 3 independent experiments.

deletion of Fnip1 leads to caspase activation and apoptosis of precursor BM B cells, a feature that can be rescued by antiapoptotic Bcl2 expression.

Discussion

FNIP1 and FNIP2 were originally isolated as folliculin interacting proteins in human cells.[7-9] Although lacking known functional domains, FNIP proteins were proposed to play a role in cellular energy sensing based on the observation that they associate with AMPK, a negative regulator of the mTOR pathway. Consistent with this view, homozygous loss of FLCN in human or mouse kidneys promotes overactivation of mTORC1 and mTORC2 leading to cell hyperproliferation and tumor development.[15] Furthermore, rapamycin treatment of kidney-targeted *Flcn* deficient mice partially rescues this phenotype.[11] However, whether folliculin works primarily through one or both FNIP proteins has been unclear. Our findings address this issue by comparing the phenotype of conditional *Flcn* to germ line deleted *Fnip1* mice. In both models we find that B-cell development past the pro-B cell stage is defective, indicating that Flcn and Fnip1 function cooperatively at least within the context of B-cell ontogeny. On the other hand, *Fnip1*$^{-/-}$ mice fail to phenocopy essential features of BHD syndrome, most particularly mTOR overactivation and uncontrolled kidney cell proliferation. Also contrary to results with *Flcn*$^{-/-}$ mice, Fnip1 deletion does not lead to early embryonic lethality. These data suggest that, at least for activities related to kidney and embryonic development, Fnip2 plays an important role. A second possibility is that Fnip proteins are functionally redundant in this regard. In favor of the latter hypothesis, FNIP1 and FNIP2 are highly homologous, displaying ~ 75% sequence similarity.[8,9] In addition, none of the BHD-associated mutations described so far targets *FNIP1* or *FNIP2* genes. Instead, most mutations disrupt folliculin's capacity to associate both with FNIP1 *and* FNIP2.[7-9] A formal test of these 2 scenarios awaits germ line deletion of *Fnip2* as well as a combined deletion of *Fnip1* and *Fnip2* in the mouse.

Another novel aspect of our studies concerns the observation that, independent of mTOR signaling, Fnip1 and folliculin control BM B-cell survival and pro-B-cell differentiation. This result was unexpected because no B cell defects have been reported so far in conjunction with BHD syndrome. At the same time, *FLCN* mutations are monoallelic in nature, and thus, analogous to *Flcn*$^{+/-}$ mice, BHD patients display normal B-cell ontogeny. In light of this discussion on Fnip1-Fnip2 functional redundancy, our findings reveal for the first time Folliculin-Fnip1 activities within the hematopoietic system that are independent of Fnip2. Whether Fnip2 can also function independently of Fnip1 remains to be determined, but based on these findings we propose that different follicullin-Fnip complexes function at multiple levels during mammalian development and kidney cancer, and that these complexes may or may not regulate the mTOR pathway.

We have shown that the *Fnip1*$^{-/-}$ pro-B cell block is not caused by defects in V(D)J recombination or failure to express a functional B-cell surface receptor in knockout cells. Particularly, enforced expression of a pre-rearranged antibody receptor only rescued development to the transitional BM B-cell stage. On the other hand, prompted by the overactivation of caspases and enhanced apoptosis observed in *Fnip1*$^{-/-}$ pre-B cells, we achieved full peripheral reconstitution on ectopic expression of Bcl2 in the B compartment, demonstrating that absence of Flcn or Fnip primarily compromises B-cell viability at a very specific stage. Future experiments will address the precise nature of this defect, which in turn might provide us with a better understanding of the tumor suppressor function of *FLCN*.

In conclusion, our studies demonstrate that folliculin works through both mTOR-dependent and independent pathways, and that it controls B lymphopoiesis together with its interacting partner Fnip1.

All sequence data are available at the NCBI GEO database under accession no. GSE38741.

Acknowledgments

The authors thank members of the Casellas and Linehan laboratories for helpful discussions; G. Gutierrez from National Institute of Arthritis and Musculoskeletal and Skin Diseases (NIAMS) genomics facility for technical assistance; James M. Simone and Jeffrey Lay for cell sorting; and Louise Cromwell for technical support with the mouse studies.

This work was supported in part by the Intramural Research Program of NIAMS and NCI, Center for Cancer Research, National Institutes of Health (NIH). This project was funded in part with federal funds from the NCI, NIH, under contract no. HHSN261200800001E.

The content of this publication does not necessarily reflect the views or policies of the Department of Health and Human Services, nor does mention of trade names, commercial products, or organizations imply endorsement by the US Government. NCI-Frederick is accredited by AAALAC International and follows the Public Health Service Policy

for the Care and Use of Laboratory Animals. Animal care was provided in accordance with the procedures outlined in the "Guide for Care and Use of Laboratory Animals" (National Research Council; 1996; National Academy Press; Washington, DC). None of the authors of this paper have a financial interest related to this work. This study made use of the high-performance computational capabilities of the Biowulf Linux cluster at the NIH (http://biowulf.nih.gov).

Authorship

Contribution: M.B., J.R.K., L.S.S., W.M.L., and R.C. designed the research; M.B., S.K., H.C.S., R.M.H., M.E.K., H.F.O., and L.S.S. performed research; M.B., H.H., Y.H., C.G.G., and P.B. contributed vital new reagents or analytical tools; M.B., J.R.K., H.-W.S., W.R., K.-R.K.-K., W.M.L., and R.C. analyzed and interpreted data; M.B., E.S., and L.T. contributed Fnip1$^{-/-}$ mice generation; and M.B., W.M.L., and R.C. wrote the paper.

Conflict-of-interest disclosure: The authors declare no competing financial interests.

Correspondence: Rafael Casellas, NIAMS, NIH, 10 Center Dr, MSC 1930, 10/13C103-D, Bethesda, MD 20892; e-mail: rafael.casellas@nih.gov; or W. Marston Linehan, NCI, NIH, 10 Center Dr, MSC 1107, 10 CRC 1-5940W, Bethesda, MD 20892; e-mail: wml@nih.gov.

References

1. Schmidt LS, Nickerson ML, Warren MB, et al. Germline BHD-mutation spectrum and phenotype analysis of a large cohort of families with Birt-Hogg-Dube syndrome. *Am J Hum Genet.* 2005; 76(6):1023-1033.
2. Nickerson ML, Warren MB, Toro JR, et al. Mutations in a novel gene lead to kidney tumors, lung wall defects, and benign tumors of the hair follicle in patients with the Birt-Hogg-Dube syndrome. *Cancer Cell.* 2002;2(2):157-164.
3. Okimoto K, Kouchi M, Matsumoto I, Sakurai J, Kobayashi T, Hino O. Natural history of the Nihon rat model of BHD. *Curr Mol Med.* 2004;4(8):887-893.
4. Vocke CD, Yang Y, Pavlovich CP, et al. High frequency of somatic frameshift BHD gene mutations in Birt-Hogg-Dube-associated renal tumors. *J Natl Cancer Inst.* 2005;97(12):931-935.
5. Hasumi Y, Baba M, Ajima R, et al. Homozygous loss of BHD causes early embryonic lethality and kidney tumor development with activation of mTORC1 and mTORC2. *Proc Natl Acad Sci U S A.* 2009;106(44):18722-18727.
6. Knudson AG, Jr. Mutation and cancer: statistical study of retinoblastoma. *Proc Natl Acad Sci U S A.* 1971;68(4):820-823.
7. Baba M, Hong SB, Sharma N, et al. Folliculin encoded by the BHD gene interacts with a binding protein, FNIP1, and AMPK, and is involved in AMPK and mTOR signaling. *Proc Natl Acad Sci U S A.* 2006;103(42):15552-15557.
8. Hasumi H, Baba M, Hong SB, et al. Identification and characterization of a novel folliculin-interacting protein FNIP2. *Gene.* 2008;415(1-2): 60-67.
9. Takagi Y, Kobayashi T, Shiono M, et al. Interaction of folliculin (Birt-Hogg-Dube gene product) with a novel Fnip1-like (FnipL/Fnip2) protein. *Oncogene.* 2008;27(40):5339-5347.
10. Inoki K, Zhu T, Guan KL. TSC2 mediates cellular energy response to control cell growth and survival. *Cell.* 2003;115(5):577-590.
11. Baba M, Furihata M, Hong SB, et al. Kidney-targeted Birt-Hogg-Dube gene inactivation in a mouse model: Erk1/2 and Akt-mTOR activation, cell hyperproliferation, and polycystic kidneys. *J Natl Cancer Inst.* 2008;100(2):140-154.
12. Hartman TR, Nicolas E, Klein-Szanto A, et al. The role of the Birt-Hogg-Dube protein in mTOR activation and renal tumorigenesis. *Oncogene.* 2009; 28(13):1594-1604.
13. Hudon V, Sabourin S, Dydensborg AB, et al. Renal tumour suppressor function of the Birt-Hogg-Dube syndrome gene product folliculin. *J Med Genet.* 2010;47(3):182-189.
14. Cash TP, Gruber JJ, Hartman TR, Henske EP, Simon MC. Loss of the Birt-Hogg-Dube tumor suppressor results in apoptotic resistance due to aberrant TGFbeta-mediated transcription. *Oncogene.* 2011;30(22):2534-2546.
15. Linehan WM, Srinivasan R, Schmidt LS. The genetic basis of kidney cancer: a metabolic disease. *Nat Rev Urol.* 2010;7(5):277-285.
16. Hong SB, Oh H, Valera VA, Baba M, Schmidt LS, Linehan WM. Inactivation of the FLCN tumor suppressor gene induces TFE3 transcriptional activity by increasing its nuclear localization. *PLoS One.* 2010;5(12):e15793.
17. Singh SR, Zhen W, Zheng Z, et al. The Drosophila homolog of the human tumor suppressor gene BHD interacts with the JAK-STAT and Dpp signaling pathways in regulating male germline stem cell maintenance. *Oncogene.* 2006;25(44):5933-5941.
18. Dymecki SM. Flp recombinase promotes site-specific DNA recombination in embryonic stem cells and transgenic mice. *Proc Natl Acad Sci U S A.* 1996;93(12):6191-6196.
19. Lewandoski M, Meyers EN, Martin GR. Analysis of Fgf8 gene function in vertebrate development. *Cold Spring Harb Symp Quant Biol.* 1997;62:159-168.
20. Guo C, Yang W, Lobe CG. A Cre recombinase transgene with mosaic, widespread tamoxifen-inducible action. *Genesis.* 2002;32(1):8-18.
21. Kuchen S, Resch W, Yamane A, et al. Regulation of microRNA expression and abundance during lymphopoiesis. *Immunity.* 2010;32(6):828-839.
22. Schlissel MS, Corcoran LM, Baltimore D. Virus-transformed pre-B cells show ordered activation but not inactivation of immunoglobulin gene rearrangement and transcription. *J Exp Med.* 1991; 173(3):711-720.
23. Hardy RR, Carmack CE, Shinton SA, Kemp JD, Hayakawa K. Resolution and characterization of pro-B and pre-pro-B cell stages in normal mouse BM. *J Exp Med.* 1991;173(5):1213-1225.
24. Pelanda R, Schwers S, Sonoda E, Torres Rm Nemazee D, Rajewsky K. Receptor editing in a transgenic mouse model: site, efficiency, and role in B cell tolerance and antibody diversification. *Immunity.* 1997;7(6):765-775.
25. Goodnow CC, Crosbie J, Adelstein S, et al. Altered immunoglobulin expression and functional silencing of self-reactive B lymphocytes in transgenic mice. *Nature.* 1988;334(6184):676-682.
26. Strasser A, Whittingham S, Vaux DL, et al. Enforced BCL2 expression in B-lymphoid cells prolongs antibody responses and elicits autoimmune disease. *Proc Natl Acad Sci U S A.* 1991;88(19): 8661-8665.